Aluminum Impurities in Silicon: Investigation of X-ray Raman Scattering in Total Reflection X-ray Fluorescence Spectroscopy

K. Baur, J. Kerner[1], S. Brennan, A. Singh and P. Pianetta

Stanford Synchrotron Radiation Laboratory, Stanford University, Stanford CA 94309
[1]ARACOR, 425 Lakeside Drive, Sunnyvale CA 94086

Abstract: **Total Reflection X-ray Fluorescence (TXRF) using Synchrotron Radiation from the Stanford Synchrotron Radiation Laboratory (SSRL) has been used to study Al impurities on Si wafer surfaces. For primary excitation energies below the Si K absorption edge an inelastic resonance scattering due to resonant x-ray Raman scattering is observed. This scattering dominates the background behavior of the Al K fluorescence line, and consequently limits the achievable sensitivity for detection of Al surface contaminants. The energy- and angle-dependence of the resonant x-ray Raman scattering has been investigated to determine the experimental conditions for which the highest sensitivity for Al can be achieved. We find that for a precise determination of the achievable sensitivity, the specific shape of the continuous Raman background has to be taken into account. Our calculations demonstrate a minimum detection limit for Al of 6 x 10^9 atoms/cm^2 for a 10,000 second count time**.

I. Introduction

Total reflection x-ray fluorescence spectroscopy (TXRF) [1] in combination with synchrotron radiation has become one of the most powerful non-destructive techniques for detection of very low concentrations of metal impurities on Si wafer surfaces [2, 3, 4, 5]. To date, SR-TXRF has achieved a remarkable sensitivity for transition metals of 3.4 x 10^7 atoms/cm^2, as determined from Fe, Ni and Zn standards [6]. Such sensitivities are required by the semiconductor industry to develop future generations of wafer cleaning technologies. Having established the TXRF technique for the analysis of transition metal impurities, the development of equally sensitive techniques for light elements with $Z < 14$ is the new challenge. According to the SEMATECH roadmap a sensitivity of 3 x 10^9 atoms/cm^2 will be needed for Na and Al [7].

The K fluorescence signals of the light elements (Kα below 1.5 keV) are about a factor of 30 smaller than the ones of the medium-Z elements due to a reduced fluorescence yield. In addition to these inherent restrictions, the detection of light elements on Si is especially difficult because of the presence of the much stronger Si substrate fluorescence signal at 1.74 keV which tends to dominate the spectrum.

These limitations can be overcome by using synchrotron radiation (SR) as the excitation source because it offers several advantages over x-ray tubes. First, SR provides a

high incident flux combined with a low divergence and a linearly polarized beam that leads to an increased fluorescence signal while reducing the elastic background. Second, by exploiting the tunability of synchrotron radiation, fluorescence from the Si substrate can be further reduced by choosing an excitation energy below the Si K absorption threshold. Sensitivities on the order of 9 x 10^9 atoms/cm^2 for Al have been demonstrated in previous studies using synchrotron radiation [8, 9, 11].

Al on Si is particularly challenging because the two respective K absorption edges are only separated by 260 eV. Thus the incident beam energy must be between these two energies in order to excite the Al Kα fluorescence but not the Si Kα. However, despite these precautions one observes a substantial increase in the background starting at about 100 eV below the primary excitation energy of 1750 eV and extending to lower energies by several hundred eV. The origin of this background is resonant x-ray Raman scattering which is an inelastic x-ray scattering process [12, 13, 14]. The first observation of this process was made by Sparks [12] using monochromatic Cu Kα radiation from an x-ray tube on different target materials. The first synchrotron radiation based experiment was performed by Eisenberger et al. [15], who investigated this process in the vicinity of the Cu K-edge resonance.

The additional background due to the x-ray Raman scattering degrades the sensitivity of the TXRF measurement defined as the minimum detection limit or MDL. The MDL is generally quantified using an elemental standard from the equation:

$$MDL = 3C\sqrt{I_{BG}} / I_{Peak} \qquad (1)$$

where C is the concentration of the elemental standard and I_{Peak} is the integrated intensity of the respective fluorescence peak minus the background intensity, I_{BG}, under that peak [16].

Furthermore, the non-symmetric shape of the x-ray Raman scattering background strongly overlaps the Al fluorescence signal resulting in fitting problems and thus affecting the accuracy of the MDL [17]. This paper contains a detailed study of the resonant x-ray Raman scattering in TXRF as a function of excitation energy and angle of incidence. It will show a method of calculating the shape of the Raman scattering profile in order to accurately determine the currently achievable MDL for Al with TXRF.

II. Experiment

The measurements were carried out at the JUMBO beamline (BL 3-3) at the Stanford Synchrotron Radiation Laboratory (SSRL). The basic experimental configuration used in this work is sketched in Fig. 1. The incoming beam is focused onto the sample by a platinum-coated fused quartz cylindrical mirror with a critical energy of 3 keV that accepts up to 10 horizontal mrad of synchrotron radiation from a bending magnet. The beam is then monochromatized by a double multilayer monochromator which uses a pair Mo - B_4C multilayers with a periodicity of 30 Å. These multilayers have been especially

designed for high reflectivity (about 20 %) between the Si-K- and Al-K edges at 1839 eV and 1559 eV, respectively. For Al analysis, the monochromator was tuned to 1750 eV because this photon energy gives a high cross section for Al while not exciting Si K fluorescence. Fig. 2 shows the calculated reflectivity for a single multilayer as a function of the photon energy as well as for a double-multilayer configuration for a Bragg angle of 6.9 ^{o}. The increase in intensity below 300 eV is due to total external reflection from the surface. The single multilayer configuration shows a 3 % reflectivity in the second order as well as a relatively strong background reflectivity. These contributions are significantly decreased by the addition of a second multilayer as demonstrated in Fig.2. After monochromatization the beam enters the chamber through a 25 μm thick Be window and strikes the wafer surface. The Be window further serves to eliminate the background below 1 keV.

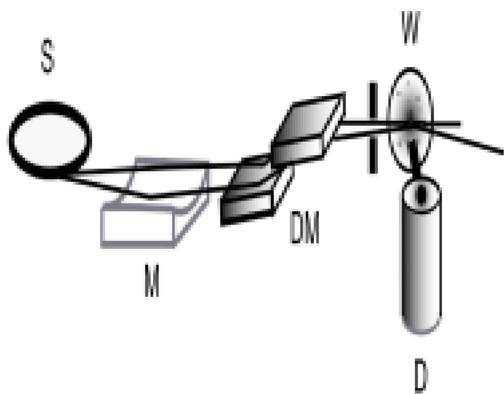

Figure 1. - Schematic representation of the experimental system used for synchrotron radiation TXRF experiments at SSRL (S). The beam is focused onto the wafer (W) by a cylindrical mirror (M) and monochromatized by a double multilayer monochromator (DM). The Si(Li) detector (D) is aligned along the polarization vector of the synchrotron radiation.

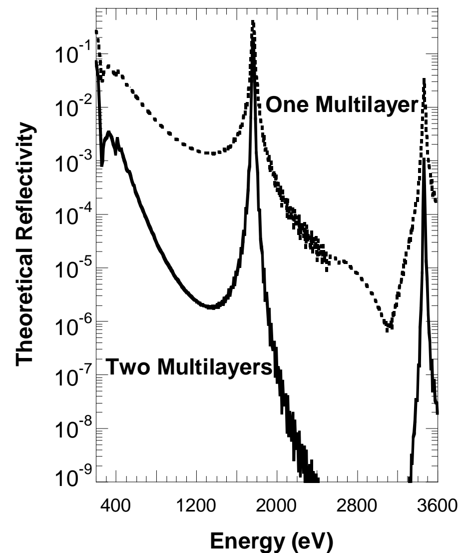

Figure 2 - Theoretical reflectivity of a single and double multilayer configuration for a Mo/B_4C multilayer with a d-spacing of 30 Å and a Bragg angle of 6.9 ^{o}.

The detector used in this experiment is an energy-dispersive Si(Li) solid state detector with a 5 μm beryllium entrance window and an active area of 10 mm^2 having an energy resolution of 130 eV for Mn Kα and 100 eV for Si Kα. A Fe-55 source was used for the energy calibration of the detector. The standard SR-TXRF configuration was used where the wafer is mounted vertically in front of and perpendicular to the detector axis which is then aligned along the polarization vector of the synchrotron radiation. This configuration allows the detector to subtend a large solid angle as well as take advantage of the reduced scattered x-ray intensity emitted in the direction of the polarization vector.

The wafer can be translated in x, y and z as well as rotated along a vertical axis perpendicular to the incoming beam to set the angle of incidence. This angle is determined by

observing the beam downstream of the wafer on a glass window coated with a phosphorescent material. Zero degrees was determined by minimizing the width of the wafer shadow on the screen. Increasing the angle of incidence results in an additional spot on the screen that is reflected from the wafer surface [9].

The behavior of the Raman background as a function of the primary energy and sample angle has been studied using standard wafers from Hewlett-Packard Co. with an intentional Al contamination of 8×10^{12} atoms/cm^2 and 3×10^{11} atoms/cm^2. Both wafers have been cross-calibrated in concentration by using Inductively Coupled Plasma Mass Spectrometry (ICP-MS) as well as conventional TXRF from a Rigaku instrument (TXRF 300) providing a W Mα line (1.78 keV) for primary excitation [10].

III. Results and Discussion

Energy dependence of resonant x-ray Raman scattering. Fig. 3 shows typical fluorescence spectra from a wafer intentionally contaminated with 8×10^{12} atoms/cm^2 of Al for various excitation energies. All spectra were collected at an angle of incidence of 0.2^{o} and measured for 1000 seconds. The individual spectra have been shifted vertically by multiples of 100 counts for clarity of presentation. The low energy peak in all the spectra is the Al Kα fluorescence signal at 1487 eV. Except for the top spectrum, the high energy peak is the signal from the elastically scattered primary photons which increases in energy between 1690 eV and 1802 eV as the excitation energy is increased between these two values. The top spectrum was taken at an excitation energy centered at 1815 eV, i.e., 25 eV below the Si K absorption edge at 1840 eV. However, since the bandwidth of the multilayer is approximately 40 eV there are enough photons at energies higher than 1840 eV to ionize the Si K electrons. Since this process has a cross-section orders of magnitude higher than that of the RRS, the Raman peak is completely dominated by the Si Kα radiation which is now the only high energy peak in the spectrum. Note, that the Si Kα fluorescence is still quite low since the intensity of the photons above 1840 eV when the primary beam is at 1815 eV is estimated to be only 4 % of the total intensity in the primary beam.

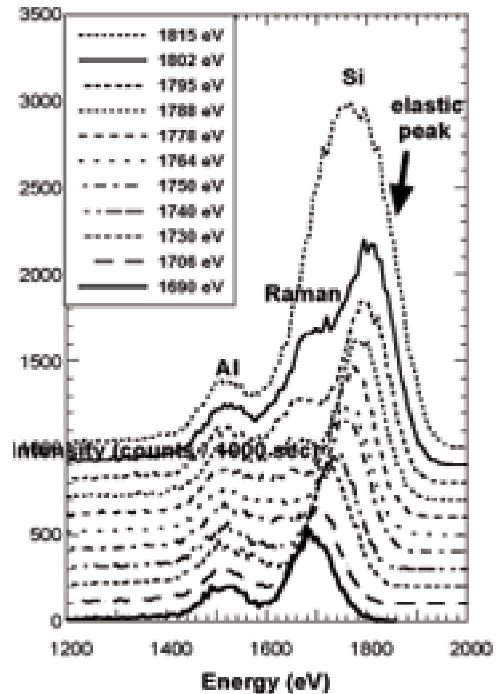

Figure 3 - TXRF spectra of a wafer intentionally contaminated with Al (concentration 8×10^{12} atoms/cm^2) for different excitation energies. This shows that the intensity of the Raman scattering becomes dominant if the energy of the incoming radiation approaches the Si K absorption edge.

Between these two peaks, all spectra except the top curve show a third structure. This is the signal caused by resonant x-ray Raman scattering (RRS), which is a reminiscent of the red shifted Stokes peak in optical Raman scattering: an incident photon is scattered inelastically, leaving the energy difference as an electronic excitation in the sample. A detailed theoretical description of the RRS process, derived from the Kramers-Heisenberg equation by time-dependent perturbation theory, can be found in Ref. [18]. Fig. 4. gives an illustration of the RRS process. The upper part of the figure shows the Raman process as known from optical spectroscopy. An outer electron is excited into an unoccupied state high above the Fermi level by absorption of a photon. This (virtual) intermediate state then decays with the electron making a transition to an unoccupied state close to the Fermi level with the energy difference being emitted as a scattered photon. The electron involved in the optical Raman scattering process is a valence electron, and the photon has an energy of only a few eV, i.e. close to the electron binding energy. On the other hand, in the x-ray case the electron belongs to an inner shell (Si L, 100 eV binding energy), and the photon energy exceeds its binding energy by an order of magnitude. The cross section for Raman scattering is therefore generally extremely low compared to elastic Rayleigh scattering. However, if the energy of the incident photon is close to an absorption threshold (i.e., the Si K edge), the Raman process is resonantly enhanced by the process shown in the lower part of Fig. 4. This inelastic scattering process is a one-step version of the well–known absorption-followed-by–emission process. A K-shell electron is excited (virtually) into an unoccupied state right above the Fermi level. Note, that this excitation is possible even for excitation energies below the K-absorption edge due to the lifetime broadening of the K shell vacancy in the final state of the absorption process. The intermediate state then decays by transition of an electron from a more shallow core level (e.g., Si L) to the K-shell vacancy, and the energy difference is emitted as the scattered photon. As both processes (Raman and inelastic scattering) have the same initial and the same final state, but different intermediate states, these two processes can resonate and enhance each other. This is demonstrated in Fig.3. The closer the energy of the incident photon is to the K shell absorption edge, i. e., the higher the absorption probability, the more intense the Raman structure is. Note, that the Raman structure is not only a single peak, but that the peak is accompanied by a low energy tail. The origin of this tailing is that a continuum of unoccupied states above the Fermi level is available for the excited electron with a transition probability that decreases exponentially as the energy of the final state above the conduction band minimum increases [19].

RRS affects the measurement of light element impurities on surfaces and limits the achievable sensitivity especially when the matrix component is just one atomic number higher than that of the element of interest as is the case for Al on Si. To excite Al K fluorescence, the incident photon energy has to be above the Al K edge. Then, however, a strong Si Raman background is superimposed on the Al

fluorescence. On the other hand, the primary photon energy must be below the Si K edge in order to suppress Si K fluorescence, which would saturate the detector as well as dominate the spectrum wiping out all other structures as discussed above. This is demonstrated in the top spectrum of Fig. 3.

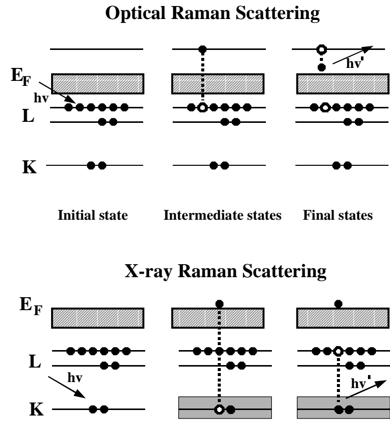

Figure 4 - Schematic energy level diagrams for Raman scattering. The upper part shows Raman scattering as it is known from optical spectroscopy, the lower part contains processes involved in resonant x-ray Raman scattering

Angular dependence of resonant x-ray Raman scattering. The amplitude of the RRS peak increases with the angle of incidence due to an increasing penetration of the primary radiation involving more Si atoms in the process. This is shown in Fig.5 where fluorescence spectra taken at an excitation energy of 1750 eV for different angles of incidence between 0.3 ^{o} and 1.2 ^{o} are plotted. The feature that dominates all spectra is the scattering of the incident synchrotron radiation at 1750 eV. At 1486 eV we find the fluorescence signature of Al. Between these two peaks all spectra again show the signal due to RRS which increases with increasing angle of incidence and becomes dominant for very large angles above the critical angle for total external reflection (0.9 ^{o} at 1730 eV). Since Raman scattering is related to the absorption of the primary radiation in the Si matrix, its signal increases with increasing angle of incidence due to the increasing penetration depth of the primary radiation. On the other hand, its contribution is low for glancing angles significantly below the critical angle where total external reflection dominates.

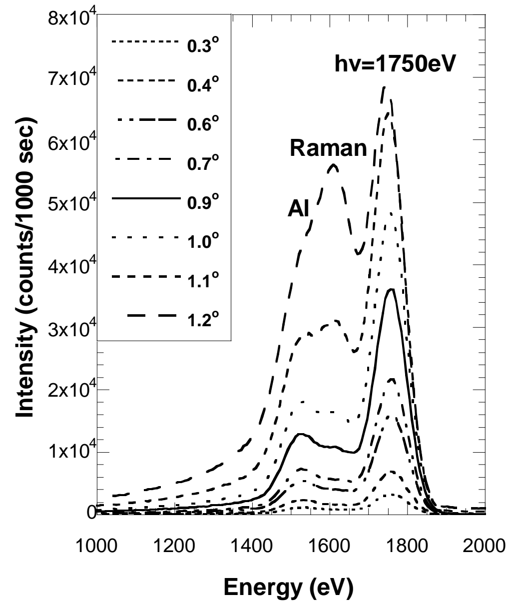

Figure 5 - Fluorescence spectra from a wafer intentionally contaminated with Al at a concentration of 8 x 10 ^{12} atoms/cm^2 as a function of the angle of incidence. The spectra show that the intensity of the resonant x-ray Raman scattering becomes dominant for large angles of incidence.

Fig. 3 and Fig. 5 demonstrate qualitatively that for best detection limits both the energy range of the exciting synchrotron radiation as well as the angle of incidence must be carefully chosen. To determine the conditions for achieving the highest sensitivity, each spectrum in Fig. 5 has been deconvolved in the energy range between 1000 eV and 2000 eV and the intensity of the Al fluorescence, the Raman

background and the scattered synchrotron radiation has been determined as a function of the angle of incidence. The lineshape of the Al fluorescence line and the elastically scattered radiation is dominated by the detector resolution, which is a Gaussian function with a fixed FWHM of 100 eV. The lineshape of the inelastic x-ray Raman scattering is described by the analytic expression for the differential cross section for x-ray Raman scattering [20, 21]

$$\frac{d^2\sigma}{dE_{Sc}d\Omega} = \frac{r_0^2}{2E_K}\left(C_1 + C_2 \cos^2\theta\right) \quad (2)$$

where E_{Sc} is the scattered x-ray energy, Ω the solid angle subtended by the detector, r_0 the classical electron radius, E_K the Si K shell absorption energy for this particular case, θ the scattering angle with respect to the linear polarization vector of the incoming synchrotron radiation and C_1 and C_2 coefficients as calculated by Gavrila [20, 21] for $\theta = 0°$.

In order to fit the data, this Raman scattering profile must be convolved with the detector broadening (FWHM: 100 eV) and multiplied by the transmission function of the 5 µm Be filter in front of the detector. The result is shown in Fig. 6 for three specific angles of incidence of 1.2 °, 0.9 ° and 0.4 °. Note, that the energy difference of 140 eV between the high-energy limit of the Raman continuum and the elastically scattered peak of the primary radiation is higher than the expected value derived from the Si L binding energy because the detector broadening causes the non-symmetric resonant Raman scattering signature to shift to a lower energy. In addition, the sum of the two fitted Gaussian functions and the Raman background is indicated in Fig. 6 as a solid line. The figure demonstrates that the theoretical modeling curve for the Raman background agrees very well with the experimental background behavior. This is especially evident in the energy range between 1000 eV and 1400 eV.

It should also be noted, that any low energy tailing due to incomplete charge collection in the detector cannot account for the shape of the Raman background. This was tested by tuning the excitation energy to a value above the Si K absorption edge. The low energy background of the now very strong Si Kα fluorescence line is an order of magnitude smaller than the inelastic Raman continuum for excitation energies below the Si K absorption edge, thus verifying that incomplete charge collection gives a negligible contribution to the background.

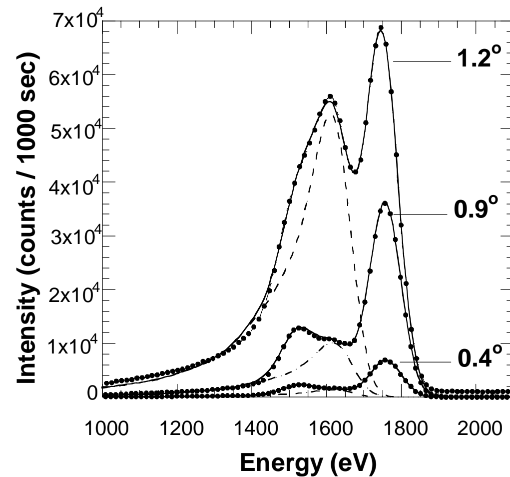

Figure 6 - Least-squares fits of the fluorescence spectra from a wafer intentionally contaminated with Al at a concentration of 8×10^{12} atoms/cm^2 for three different angles of incidence including the measured data (dots) , the fitted Raman background (- - -) and the sum of all contributions as a solid line.

Fig. 7 shows the intensity of the Al Kα fluorescence line, the Raman background and the elastically scattered primary radiation as a function of the angle of incidence as determined from the fits from Fig. 6. The data were taken up to a maximum angle of 1.2 ^{o} beyond which the detected count rate saturated. The experimental uncertainty in the determination of the angle of incidence is estimated to be $\pm 0.1^o$. The figure shows that the intensity of the Raman and scatter signals both increase with increasing angle of incidence because they both depend on the penetration depth into the substrate. On the other hand, the fluorescence signal increases up to the critical angle whereupon it reaches a maximum value. Theoretically, the fluorescence intensity is expected to decrease above the critical angle [22] whereas the scattered and Raman signals continue to increase.

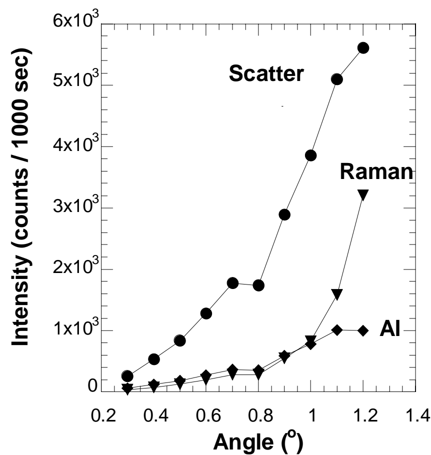

Figure 7 - Dependence of the intensity of the elastically scattered radiation, Raman background and Al fluorescence signal on the angle of incidence.

Using the angular dependence of the Raman scattering background and the Al signal intensity the MDL is calculated as a function of the incident angle according to equation (1). The result in Fig. 8 shows, that the given MDL continuously decreases for increasing angles of incidence up to the critical angle, resulting in a best MDL of 2.8 x 10^{10} atoms/cm^2 right at the critical angle.

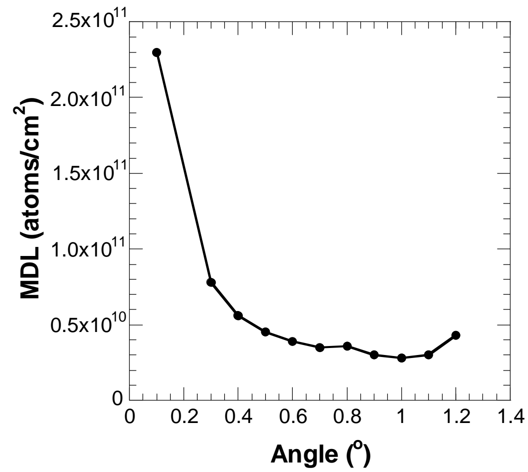

Figure 8 - Dependence of the minimum detection limit on the angle of incidence for a 1000 second count time.

In order to further explore the limits of detection, a standard wafer with a substantially lower Al contamination level of 3 x 10^{11} atoms/cm^2 was also studied. Fig. 9 shows the fluorescence spectrum (dots) taken with an excitation energy of 1730 eV and an angle of incidence of 0.1^o for 10,000 seconds count time along with the fitted contributions from the elastically scattered signal, the Al Kα line and the Raman background. The MDL under these conditions is 6.0 x 10^9 atoms/cm^2. These conditions were originally chosen because the fluorescence spectrum of Fig. 9 showed a very good peak to valley ratio and thus appeared that it would give the best MDL. However, upon the subsequent analysis leading to Fig. 8, it is now clear that an improved MDL by up to a factor of

8 could be achieved by increasing the incident angle closer to the critical angle. Thus, although the Raman background will increase with the angle of incidence, it contributes to the MDL only as the square root whereas the Al signal which is also increasing contributes linearly to the MDL resulting in an overall improvement. This will be exploited in the near future, and should result in a MDL of about 7.5 x 10^8 atoms/cm^2 for a 10,000 second count time. This corresponds to 2.4 x 10^9 atoms/cm^2 for a standard 1000 second count time. Note, that even the MDL achieved so far is much lower than what can currently be achieved (5 x 10^{10} atoms/cm^2) by conventional TXRF using a rotating anode.

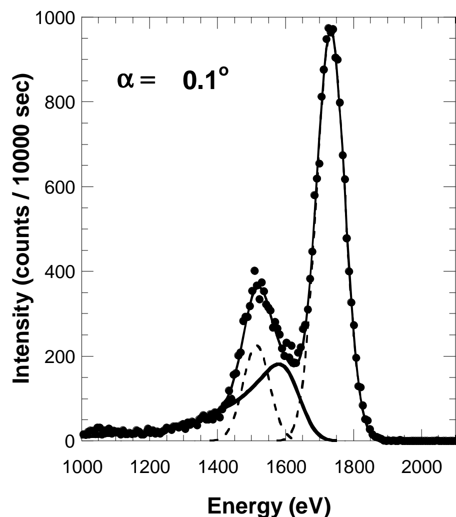

Figure 9 - Fluorescence spectrum from a wafer intentionally contaminated with Al at a concentration of 3 x 10^{11} atoms/cm^2 (dots). In addition the modeled profile of the x-ray Raman scattering including detector broadening is shown (—), as well as the Gaussian fits for the pure Al signal and the elastic scattering (---). The sum of the Gaussian fit and the Raman profile representing the simulated spectrum is shown as a solid line.

IV. Conclusion

We have shown that by tuning the excitation energy below the Si K absorption threshold, the Si K fluorescence can be decreased at the expense of a substantial increase in backgroundwhich ultimately limits the overall sensitivity of TXRF for low Z elements. By studying its energy- and angle dependence, this background has been attributed to inelastic x-ray Raman scattering. By deconvolution of the spectra, we demonstrate that in spite of the occurrence of inelastic x-ray Raman scattering, good detection limits can still be achieved. Furthermore, the MDL as a function of the angle of incidence has been calculated. The results show, that the MDL for Al can be further reduced to about 7.5 x 10^8 atoms/cm^2 for a 10,000 second count time with the angle of incidence at the critical angle for total external reflection. Note, that the experimentally achieved MDL of 6 x 10^9 atoms/cm^2 is better than what is currently achievable by conventional TXRF using a rotating anode. This demonstrates that TXRF in combination with Synchrotron Radiation is a powerful technique for the detection of low Z impurities on Si wafer surfaces.

Acknowledgement

We would like to thank the staff of SSRL for their expert technical assistance and especially A. Fischer-Colbrie of Hewlett-Packard Co. for providing the Al standards.

This work was performed at SSRL, which is supported by the Department of Energy, Office

of Basic Energy Science. In addition, KB and PP acknowledge the support of NSF under the STTR program.

References

1. R. Klockenkämper, *Total Reflection X-ray Fluorescence Analysis,* Chemical Analysis **140**, John Wiley & Sons, Inc., New York (1997).

2. P. Pianetta, N. Takaura, S. Brennan, W. Tompkins, S. S. Laderman, A. Fischer-Colbrie, A. Shimazaki, K. Miyazaki, M. Madden, D. C. Wherry, J. B. Kortright, Rev. Sci. Instrum. **66**, 1293 (1995).

3. F. Comin, M. Navizet, P. Mangiagalli, G. Apostolo, Nucl. Instrum. Meth. **B 150**, 538 (1999).

4. S. Brennan, P. Pianetta, S. Gosh, N. Takaura, C. Wiemer, A. Fischer-Colbrie, S. Laderman, A. Shimazaki, A. Waldhauer, M. A. Zaitz, in Application of Synchrotron Radiation Techniques to Materials Science IV **542**, ed. S. M. Mini, D. L. Perry, S.R. Stock, L. J. Terminello, MRS, Boston (1998).

5. A. Iida, A. Yoshinaga, K. Sakurai, Y. Gohshi, *Anal. Chem.* **58**, 394 (1986).

6. P. Pianetta, K. Baur, S. Brennan, D. Werho, J. Wang, accepted in Thin Solid Films.

7. SEMATECH roadmap meteorology, http://notes.sematech.org/1997pub.htm.

8. S. Brennan, W. Tompkins, N. Takaura, P. Pianetta, S. S. Laderman, A. Fischer-Colbrie, J. B. Kortright, M. C. Madden, D. C. Wherry, Nucl. Instrum. Meth. **347**, 417 (1994).

9. M. C. Madden, D. C. Wherry, P. Pianetta, S. Brennan, Materials Research Society: Pittsburgh, 125 (1993).

10. Rigaku, TXRF 300, Q. Zhu, B. Burrow, Accurel Systems International, Sunnyvale (CA), private communication.

11. N. Takaura, *Synchrotron Radiation Total Reflection X-ray Fluorescence of Silicon Wafer Surface*, Department of Materials Science and Engineering, Thesis, Stanford University (1997).

12. C. J. Sparks, Phys. Rev. Lett. **33,** 262 (1974).

13. T. Aberg, B. Crasemann, in *Resonant Anomalous X-Ray Scattering Theory and Applications,* ed. G. Materlik, C. J. Sparks, K. Fischer, Elsevier Science (1994).

14. F. Gel'mukhanov, H. Agren, Physics Reports **312**, 87 (1999).

15. P. Eisenberger, P. M. Platzman, H. Winick, Phys. Rev. Lett. **36**, 623 (1976).

16. E. P. Bertin, *Principles and Practice of X-Ray Spectrometric Analysis*, New York, Plenum Press, 1975.

17. C. Streli, P. Kregsamer, P. Wobrauschek, H. Gatterbauer, P. Pianetta, S. Pahlke, L. Fabry, L. Palmetshofer, M. Schmeling, Spectrochim. Acta **54B**, 1433 (1999).

18. J.J Sakurai, *Advanced Quantum Mechanics*, Adison-Wesley, London (1967).

19. J. M. Jaklevic, R. D. Giauque, A. C. Thompson, Anal. Chem. **60**, 483 (1988).

20. M. Gavrila, M. N. Tugulea, Rev. Roum. Phys. **20**, 209 (1975).

21. M. Gavrila, Rev. Roum. Phys. **19**, 473 (1974).

22. U. Weisbrod, R. Gutschke, J. Knoth, H. Schwenke, Fresenius Z. Anal. Chem. **83**, 341 (1991).